ChemPubSoc Europe

DOI: 10.1002/cctc.201600120

CHEMCATCHEM Communications

Pillared Sn-MWW Prepared by a Solid-State-Exchange Method and its Use as a Lewis Acid Catalyst

Limin Ren[+],[a] Qiang Guo[+],[a] Marat Orazov,[b] Dandan Xu,[a] Dorothea Politi,[d] Prashant Kumar,[a] Saeed M. Alhassan,[c] K. Andre Mkhoyan,[a] Dimitrios Sidiras,[d] Mark E. Davis,[b] and Michael Tsapatsis*[a]

Pillared Sn-MWW (Sn-MWW(SP)-SSE) was prepared through a solid-state-exchange (SSE) route. The pillared structure was inherited from pillared B-MWW, and Sn was inserted in the framework by boron leaching and solid-state-exchange with tin tetrachloride pentahydrate. The Sn-MWW(SP)-SSE with framework Sn sites exhibits Lewis acidity and good catalytic performance for the Baeyer–Villiger oxidation, and mono- and disaccharide isomerizations.

Zeolites[1–3] are important heterogeneous acid catalysts. Among them, there is a set with structures consisting of lamellar sheets.[4] These 2-dimensional (2D) layered zeolites, which can be manipulated by calcination, swelling, pillaring, or exfoliation (delamination), are regarded as promising catalysts for reactions involving bulky molecules.[4–7] Swelling followed by delamination or pillaring are routes for creating mesoporosity in between the 2D layers. Generally, swelling is a step performed to expand the inter-layer spacing; it is achieved by using long chain surfactants that interact with the silanols between the layers.[4,7] Usually, this step may be performed under aggressive conditions, which may lead to partial dissolution and destruction of the layers. Delamination or exfoliation is performed after swelling to obtain individual layers or few-layer stacks.[7–10] Compared with delamination, pillaring leads to a more uniform and ordered structure.[11] It is performed by placing oxide pillars between adjacent layers to create mesopores.[7]

Pillared MWW in its aluminosilicate form (called MCM-36) was first introduced in the 1990s by pillaring the layered precursor (MCM-22(P)) in an effort to combine the Brønsted acidity of zeolites with accessibility to bulky molecules.[7] Since then, numerous studies have attempted the structural characterization of pillared aluminosilicate MWW and to find its correlation with catalytic activity.[11,12] To obtain pillared layered materials with highly crystalline layers, the conditions under which the swelling step is performed are decisive and should be well-controlled. For example, mild swelling of MCM-22(P) results in a pillared material with improved structural preservation of the 2-dimensional MWW layers, which has been correlated with improved catalytic performance.[13]

As a Lewis acid catalyst,[14–21] Sn-MWW has attracted attention from both the synthetic and catalytic perspectives. Hensen et al. developed a "re-growth" method for preparing Sn-MWW, which was highly active for the conversion of trioses to methyl lactate and lactic acid.[14] Hydrothermal synthesis of Sn-MWW and its transformation to an MCM-56 analog were reported by Wu's group.[15a] Zones et al. studied delaminated Sn-MWW as an effective solid Lewis acid catalyst for the Baeyer–Villiger oxidation.[15b]

Here, we present the preparation of pillared Sn-MWW with well-preserved intra-layer crystallinity and compare its performance with that of other catalysts for the Baeyer–Villiger oxidation and mono- and disaccharide isomerizations. Table 1 lists the zeolite samples prepared in this study. Detailed information regarding their synthesis can be found in the Supporting Information.

Swelling of the layered precursor, B-MWW(Pr), was performed under mild conditions to avoid destruction of the intra-layer crystallinity. As shown by the XRD patterns in Figure 1 A, traces a and b, the (0 0 1) peak shifted from $2\theta = 3.25$ to 2.5°, corresponding to an increase in layer spacing. Intra-layer peaks (2 2 0) and (3 1 0) are clearly observed in the swollen material, indicating that the crystallinity of the layers was preserved.[13] Figure 1 A, trace c, shows the XRD pattern of the pillared material, B-MWW(SP). The low-angle (0 0 1) peak at $2\theta = 2.06°$ (corresponding to a *d* spacing of 43 Å, which is characteristic of MCM-36) indicates that B-MWW(SP) is successfully pillared. The (0 0 2) and (0 0 3) peaks reflect ordered inter-layer stacking. In the wide-angle range, the (1 0 0), (2 2 0), and (3 1 0)

[a] Dr. L. Ren,[+] Dr. Q. Guo,[+] D. Xu, P. Kumar, Prof. K. A. Mkhoyan, Prof. M. Tsapatsis
Department of Chemical Engineering and Materials Science
University of Minnesota
421 Washington Avenue SE
Minneapolis, MN, 55455 (USA)
E-mail: tsapatsis@umn.edu

[b] M. Orazov, Prof. M. E. Davis
Chemical Engineering
California Institute of Technology
Pasadena, CA, 91125 (USA)

[c] Prof. S. M. Alhassan
Department of Chemical Engineering
The Petroleum Institute, Abu Dhabi (UAE)

[d] Dr. D. Politi, Prof. D. Sidiras
Laboratory of Simulation of Industrial Processes
Department of Industrial Management and Technology
University of Piraeus
80 Karaoli & Dimitriou
GR-18534 Piraeus (Greece)

[+] These two authors contributed equally.

Supporting information and the ORCID identification number(s) for the author(s) of this article can be found under http://dx.doi.org/10.1002/cctc.201600120.

Table 1. Nomenclature and description of synthesized materials.

Samples	Description
B-MWW(Pr)	B-MWW layered precursor, Si/B = 13
B-MWW(3D)	3D B-MWW obtained by calcination of B-MWW(Pr), Si/B = 13
B-MWW(S)	Swollen B-MWW obtained by swelling of B-MWW(Pr) with surfactant
B-MWW(SP)	Pillared B-MWW obtained by swelling and pilling of B-MWW(Pr)
De-B-MWW(SP)	De-boronated, pillared B-MWW obtained by acid leaching of the B-MWW(SP)
Sn-MWW(SP)-SSE	Pillared Sn-MWW with Si/Sn = 125 obtained from De-B-MWW(SP) by the SSE method
Sn-MWW(Pr)	Sn-MWW layered precursor, Si/Sn = 94
Sn-MWW(3D)	3D Sn-MWW obtained by calcination of Sn-MWW(Pr), Si/Sn = 94
Sn-BEA-F	Sn-BEA prepared by a fluoride-based hydrothermal synthetic method, Si/Sn = 125

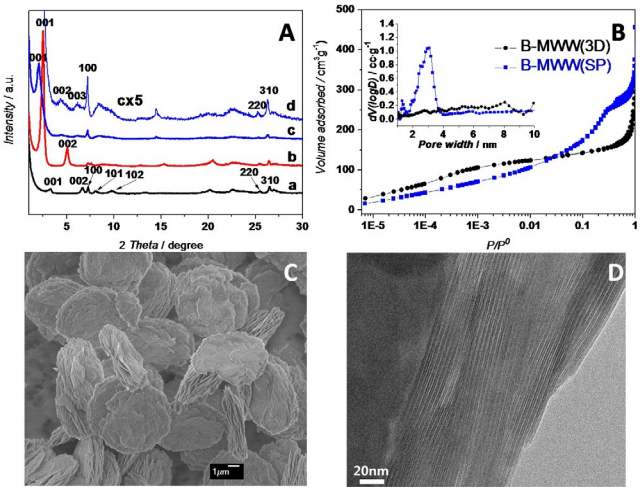

Figure 1. A) XRD patterns of B-MWW(Pr) (trace a), B-MWW(S) (trace b), B-MWW(SP) (traces c and d. The intensity of trace d is increased five-times compared with that in trace c); B) Ar adsorption/desorption isotherms of B-MWW(3D) and B-MWW(SP) (inset shows pore-size-distributions obtained by using non-local (NL)-DFT);[22] C) SEM image and D) TEM image of B-MWW(SP).

reflections are retained (Figure 1 A, trace d), suggesting preservation of the intra-layer structure.

The argon adsorption (Figure 1 B) isotherm indicates a pore size distribution centered around 3.0 nm for the pillared sample, whereas no such peak was detected in the mesopore range for B-MWW(3D). The SEM image of B-MWW(SP) shows that the original morphology of B-MWW(Pr), as seen in Figure S1 in the Supporting Information, was retained (Figure 1 C). The TEM image of B-MWW(SP) shows regularly spaced layers with high crystallinity (Figure 1 D).

After swelling and pillaring, the 12 membered ring (MR) MWW semi-cups, which are present on the external surface of MWW layers, will be accessible through the mesopores. For Sn incorporation using the solid-state-exchange (SSE) approach shown in Scheme S1 (in the Supporting Information), first boron removal from B-MWW(SP) was performed by acid treatment[14] and then SSE Sn insertion was performed by contacting with tin tetrachloride pentahydrate followed by high temperature calcination.[16a] Figure S2 (in the Supporting Information) shows the XRD patterns of B-MWW(SP), De-B-MWW(SP), and Sn-MWW(SP)-SSE, indicating that the pillared arrangement and intra-layer order were retained after acid leaching and the SSE process. Figures S3 A and S3 B (in the Supporting Information) show the SEM and TEM images of Sn-MWW(SP)-SSE, showing plate morphology and an ordered stacking of crystalline layers. As expected, Ar adsorption (Figure S4 in the Supporting Information) of Sn-MWW(SP)-SSE compared with Sn-MWW(3D) is lower at low pressures and higher at high pressures.

The diffuse reflectance UV/visible (DR-UV/vis) spectrum of Sn-MWW(SP)-SSE exhibits a main peak centered at 205 nm (Figure S5 in the Supporting Information), which is assigned to the tetrahedrally coordinated Sn species.[15b,23a] The Lewis acidic properties of Sn-MWW(SP)-SSE were probed with adsorption of deuterated acetonitrile, followed by FTIR spectroscopy (Figure 2 A). C–N stretching vibration peaks corresponding to physisorbed ($\approx$2261 cm^{-1}), silanol-bound ($\approx$2273 cm^{-1}), and Lewis-acid-bound ($\approx$2305 cm^{-1}) deuterated acetonitrile are evident.[23] Similar C–N stretching vibrations of adsorbed deuterated acetonitrile were also observed for Sn-MWW(3D) as shown in Figure 2 C. The IR spectra of pyridine adsorbed on Sn-MWW(SP)-SSE after evacuation at different temperatures are shown in Figure 2 B. In addition to the bands attributed to Lewis acid sites (1449, 1489, 1607, and the shoulder peak 1613 cm^{-1}), there are bands (1489, 1543, and faint peak 1636 cm^{-1}) corresponding to pyridine adsorbed on Brønsted acid sites.[14,24] Loss of the intensity after evacuation at 350 °C, suggests a weaker Brønsted acidity than that associated with Al Brønsted acid sites.[24] The weak Brønsted acidity was also observed in Sn-MWW(3D) (Figure 2 D). The Brønsted acidity of both samples can be attributed to boron remaining after acid leaching. Ratios of Si/B $\approx$ 200 for Sn-MWW(3D) and Si/B $\approx$ 300 for Sn-MWW(SP)-SSE, determined by inductively coupled plasma optical emission spectrometry (ICP-OES), further support this hypothesis.

Sn-MWW(SP)-SSE was tested as a catalyst for the Baeyer–Villiger oxidation of the cyclic ketone 2-adamantanone and compared with various zeolite catalysts (Table 2, Table S1 in the Supporting Information). There is no lactone produced over bulk Sn-MFI,[25] as the 10 MR channels are too small to accommodate 2-adamantanone, which has an estimated size of 7.0 Å.[26] Sn-MWW(3D) shows 49.4% conversion and 48.2% yield of lactone after 4 h reaction. The activity is mainly attributed to Sn sites located on the external surface as the intra-layer 10 MR should not be accessible to such bulky molecules and the large super cage (with an inner diameter of approxi-

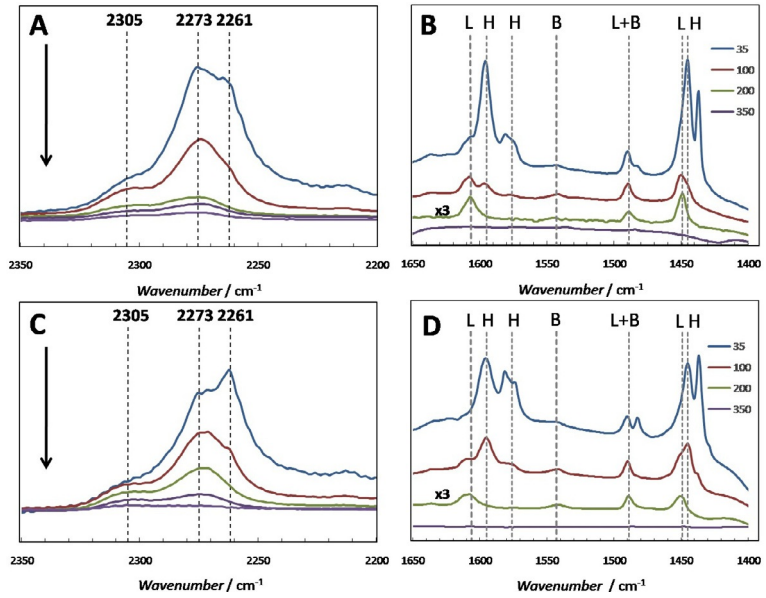

Figure 2. FTIR spectra of deuterated acetonitrile adsorbed on A) Sn-MWW(SP)-SSE and C) Sn-MWW(3D). The arrows indicate the desorbing sequence of deuterated acetonitrile in vacuo. FTIR spectra after pyridine adsorption and evacuation at different temperatures on B) Sn-MWW(SP)-SSE and D) Sn-MWW(3D). The 200 °C spectra are multiplied by a factor of three to enhance the visibility of the peaks. Absorption band characteristics for specifically adsorbed pyridine are denoted by H for hydrogen-bonded pyridine, B for adsorption on Brønsted sites, and L for Lewis acid sites.

Table 2. Baeyer–Villiger oxidation of 2-adamantanone catalyzed by different catalysts.[a]

Catalysts	Si/Sn	Conversion [%]	Yield [%]	Selectivity [%]
Sn-MWW(3D)	94	49.4	48.2	97.6
Sn-MWW(SP)-SSE	125	90.5	85.1	94.0
Sn-BEA-F	125	82.3	79.4	96.5
Sn-MFI	125	< 3	–	–

[a] Reaction conditions: ketone 1 mmol, 30 wt% H_2O_2 1.5 mmol, Sn/ketone = 0.66%, dioxane 3.09 g, 90 °C, 4 h.

mately 7.1 Å and height of approximately 18.2 Å) can only be reached through the 10 MR channels.[5,27] As expected, Sn-MWW(SP)-SSE shows much higher activity (90.5% conversion and 85.1% yield of lactone) than that of Sn-MWW(3D). Furthermore, Sn-MWW(SP)-SSE shows even better catalytic performance when compared with that of the state-of-art catalyst Sn-BEA-F (82.3% conversion and 79.4% yield of lactone).

To further explore the active sites of Sn-MWW catalysts and their accessibility, mono- and disaccharide isomerizations involving larger molecules were investigated. Glucose (GLU) isomerization was performed in ethanol by following the reaction sequence reported in ref. [28]. According to this procedure (Scheme S2 in the Supporting Information), GLU is first reacted to produce a mixture of fructose (FRU; GLU isomerization product) and ethyl fructoside (FRU ketalization product with alcohol). Upon addition of water, hydrolysis of the fructoside yields FRU.[28,29] With this approach, the FRU yield could be increased compared with that achieved by isomerization in water. By performing GLU isomerization in this way, both Sn-MWW(3D) and Sn-MWW(SP)-SSE have shown high FRU yield (> 50%) and high FRU selectivity (around 70%) at similar GLU conversions of around 75% (Figure 3, Figure S6 in the Supporting Information) after 24 h of the reaction. This is comparable to the previously reported performance of Sn-SPP and much higher than that of Sn-BEA-F (Table S2 in the Supporting Information).[29] As can be seen from Figure 3, the yield of fructose on Sn-MWW(SP)-SSE exceeds 50% after about 8 h, whereas with Sn-MWW(3D), it reaches comparable levels after 24 h. It is reasonable to attribute this difference to the alleviated diffusion limitations on Sn-MWW(SP)-SSE compared with Sn-MWW(3D), as similar acidic properties of the two catalysts have been confirmed by FTIR, and the reaction appears to proceed with a similar mechanism in both catalysts as discussed next.

The isotopic identity (H or D) at the C1 position was determined by ^{13}C NMR spectroscopy for fructose generated through glucose isomerization catalyzed by Sn-MWW(SP)-SSE in methanol with inverse isotopic enrichment at the C2 position of the starting glucose (e.g., for glucose with natural abundance H at C2, the reaction was run in [D_4]MeOH). No isotopic scrambling with the solvent was observed (Figures S7, S8 in the Supporting Information), strongly suggesting that this isomerization proceeds primarily through a 1,2-intramolecular hydride shift that has been associated with the framework Lewis acidic "open" Sn sites in Sn-BEA,[30] rather than through an enolization mechanism that prevails on SnO_2 and homogeneous bases in methanol.[31,32] Similarly, it is demonstrated that in the presence of Sn-MWW(3D), the isomerization reaction proceeds by way of an intramolecular hydride shift (Figures S7, S8).[30–32]

We also tested the long-term stability of the Sn-MWW(SP)-SSE catalyst by performing reactions over recycled and calcined catalysts. It was found that the catalyst retains its glu-

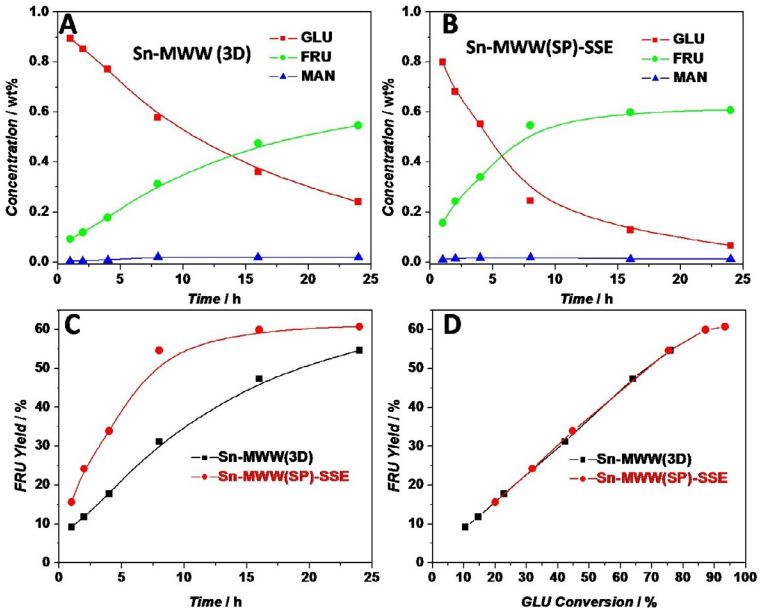

Figure 3. A and B) GLU isomerization reaction profiles as a function of time. A) Sn-MWW(3D) and B) Sn-MWW(SP)-SSE as catalyst. C and D) FRU yield versus reaction time and FRU yield versus GLU conversion over different catalysts. Reaction conditions: 1 wt% GLU (0.05 g) in ethanol (4.95 g), GLU/Sn = 74, 90 °C. After quenching the reactor in an ice bath, 6.45 g of deionized water was added to hydrolyze the ethylated sugars at 90 °C for 24 h. The fructose and mannose (MAN) concentrations and yields were obtained after the indicated reaction time followed by hydrolysis. Reaction time is the time for reaction in ethanol before the addition of water (see the Supporting Information).

cose isomerization activity after at least five runs (Figure S9 in the Supporting Information). Moreover, the ordered layer structure and intra-layer crystallinity of the used zeolite catalyst after the fifth run are still preserved as confirmed by XRD and Ar adsorption/desorption isotherms (Figure S10 in the Supporting Information).

Next, maltose, which is a much larger molecule, was also used as the isomerization substrate to probe the accessibility of the active sites of the Sn-BEA-F and Sn-MWW catalysts. Similarly to GLU isomerization, when maltose (MAL) to maltulose (MALTU) isomerization was performed in alcohols (such as ethanol and *n*-propanol), intermediates, which can be converted back to the isomerized sugar through a hydrolysis step, were observed (Scheme S3 in the Supporting Information). As presented in Table 3, after 24 h of reaction, Sn-BEA-F shows MAL conversion of 8.9% in ethanol and 8.0% in *n*-propanol, which are much lower than that of Sn-MWW(3D) (40.5% conversion, 33.6% yield in ethanol and 38.9% conversion, 28.9% yield in *n*-propanol) and Sn-MWW(SP)-SSE (79.4% conversion, 61.1% yield in ethanol and 75.6% conversion, 59.1% yield in *n*-propanol). Compared with Sn-MWW(3D), Sn-MWW(SP)-SSE shows higher MALTU yields both in ethanol and *n*-propanol (Table 3).

Table 3. Maltose isomerization to maltulose over different catalysts.[a]

Catalysts	Solvent	Conversion [%]	Yield [%]	Selectivity [%]
Sn-BEA-F	ethanol	8.9	6.7	75.3
Sn-MWW(3D)	ethanol	40.5	33.6	83.0
Sn-MWW(SP)-SSE	ethanol	79.4	61.1	77.0
Sn-BEA-F	*n*-propanol	8.0	6.1	76.3
Sn-MWW(3D)	*n*-propanol	38.9	28.9	74.3
Sn-MWW(SP)-SSE	*n*-propanol	75.6	59.1	78.2

[a] Reaction conditions: 1 wt% maltose in 3 g of alcohol (ethanol or *n*-propanol) at 90 °C for 24 h. Sn/MAL = 1/35. After quenching the reactor in an ice bath, 4 g of deionized water was added to perform the hydrolysis at 90 °C for 48 h. The MALTU yields are those obtained after the reaction time of 24 h and 48 h of hydrolysis at 90 °C.

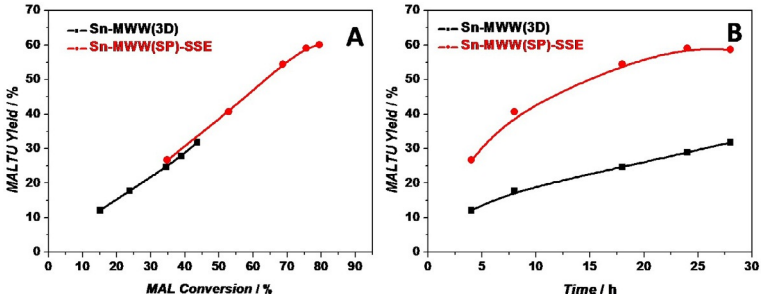

Figure 4. Isomerization of MAL to MALTU in *n*-propanol. A) MALTU yield versus MAL conversion and B) MALTU yield versus reaction time over Sn-MWW(3D) and Sn-MWW(SP)-SSE. Reaction time is the time for reaction in *n*-propanol before the addition of water (see the Supporting Information).

For a more detailed comparison of the catalytic performance of these two materials, the reaction in *n*-propanol was followed as a function of time. Sn-MWW(SP)-SSE exhibits higher MAL conversion and MALTU yield over all the reaction times (4 h to 30 h) but both materials show similar selectivity and their yield versus conversion curves overlap and complement each other (Figure 4).

In conclusion, it was demonstrated that mesoporous pillared Sn-MWW (Sn-MWW(SP)-SSE) with ordered inter-layer stacking and preserved intra-layer crystallinity was obtained through a solid-state-exchange method. It was found to be an active and regenerable catalyst for the Baeyer–Villiger oxidation and mono- and disaccharide isomerization, and, in certain cases, superior to other Sn-based zeolites.

Acknowledgements

This work was supported as part of the Catalysis Center for Energy Innovation, an Energy Frontier Research Center funded by the U.S. Department of Energy, Office of Science, Basic Energy Sciences under Award DE-SC0001004. Q.G.'s postdoctoral fellowship was partially supported by the Petroleum Institute of Abu Dhabi.

Keywords: isomerization · layered materials · Lewis acids · solid-state-exchange · zeolites

[1] a) J. Čejka, A. Corma, S. I. Zones, *Zeolites and Catalysis Synthesis Reactions and Applications*, Wiley-VCH, Weinheim, **1996**, pp. 1–57; b) H. van Bekkum, E. M. Flanigen, J. C. Jansen, *Introduction to Zeolite Science and Practice*, Elsevier, Amsterdam, **1991**, pp. 5–10; c) R. Xu, W. Pang, J. Yu, Q. Huo, J. Chen, *Chemistry of Zeolite and Related Porous Materials*, Wiley, Singapore, **2007**, pp. 1–6; d) R. M. Barrer, *Hydrothermal Chemistry of Zeolites*, Academic Press, London, **1982**, pp. 1–10.

[2] a) A. Corma, *Chem. Rev.* **1995**, *95*, 559–614; b) M. E. Davis, *Nature* **2002**, *417*, 813–821; c) C. S. Cundy, P. A. Cox, *Chem. Rev.* **2003**, *103*, 663–702; d) M. E. Davis, *Chem. Mater.* **2014**, *26*, 239–245.

[3] a) X. Zhang, D. Liu, D. Xu, S. Asahina, K. A. Cychosz, K. V. Agrawal, Y. Al Wahedi, A. Bhan, S. Al Hashimi, O. Terasaki, M. Thommes, M. Tsapatsis, *Science* **2012**, *336*, 1684–1687; b) M. Choi, K. Na, J. Kim, Y. Sakamoto, O. Terasaki, R. Ryoo, *Nature* **2009**, *461*, 246–250.

[4] a) U. Díaz, A. Corma, *Dalton Trans.* **2014**, *43*, 10292–10316; b) B. Marler, H. Gies, *Eur. J. Mineral.* **2012**, *24*, 405–428; c) W. J. Roth, P. Nachtigall, R. E. Morris, J. Čejka, *Chem. Rev.* **2014**, *114*, 4807–4837; d) M. Tsapatsis, *AIChE J.* **2014**, *60*, 2374–2381.

[5] a) M. E. Leonowicz, J. A. Lawton, S. L. Lawton, M. K. Rubin, *Science* **1994**, *264*, 1910–1913; b) P. Ayrault, J. Datka, S. Laforge, D. Martin, M. Guisnet, *J. Phys. Chem. B* **2004**, *108*, 13755–13763.

[6] a) Y. X. Wang, H. Gies, B. Marler, U. Müller, *Chem. Mater.* **2005**, *17*, 43–49; b) T. Ikeda, Y. Akiyama, Y. Oumi, A. Kawai, F. Mizukami, *Angew. Chem. Int. Ed.* **2004**, *43*, 4892–4896; *Angew. Chem.* **2004**, *116*, 5000–5004.

[7] a) C. T. Kresge, W. J. Roth, K. G. Simmons, J. C. Vartuli, WO 92/11934, **1992**; b) C. T. Kresge, W. J. Roth, U.S. Patent 5266541, **1993**; c) C. T. Kresge, W. J. Roth, U.S. Patent 5278115, **1994**.

[8] a) A. Corma, V. Fornes, S. B. Pergher, Th. L. M. Maesen, J. G. Buglass, *Nature* **1998**, *396*, 353–356; b) K. Varoon, X. Zhang, B. Elyassi, D. D. Brewer, M. Gettel, S. Kumar, J. A. Lee, S. Maheshwari, A. Mittal, C.-Y. Sung, M. Cococcioni, L. F. Francis, A. V. McCormick, K. A. Mkhoyan, M. Tsapatsis, *Science* **2011**, *334*, 72–75; c) P. Wu, D. Nuntasri, J. Ruan, Y. Liu, M. He, W. Fan, O. Terasaki, T. Tatsumi, *J. Phys. Chem. B* **2004**, *108*, 19126–19131; d) A. Corma, V. Fornés, J. Martínez-Triguero, S. B. Pergher, *J. Catal.* **1999**, *186*, 57–63.

[9] a) I. Ogino, M. M. Nigra, S.-J. Hwang, J.-M. Ha, T. Rea, S. I. Zones, A. Katz, *J. Am. Chem. Soc.* **2011**, *133*, 3288–3291; b) I. Ogino, E. A. Eilertsen, S.-J. Hwang, T. Rea, D. Xie, X. Ouyang, S. I. Zones, A. Katz, *Chem. Mater.* **2013**, *25*, 1502–1509.

[10] X. Ouyang, S.-J. Hwang, R. C. Runnebaum, D. Xie, Y.-J. Wanglee, T. Rea, S. I. Zones, A. Katz, *J. Am. Chem. Soc.* **2014**, *136*, 1449–1461.

[11] a) W. J. Roth, C. T. Kresge, J. C. Vartuli, M. E. Leonowicz, A. S. Fung, S. B. McCullen, *Stud. Surf. Sci. Catal.* **1995**, *94*, 301–308; b) Y. J. He, G. S. Nivarthy, F. Eder, K. Seshan, J. A. Lercher, *Microporous Mesoporous Mater.* **1998**, *25*, 207–224.

[12] S. Laforge, P. Ayrault, D. Martin, M. Guisnet, *Appl. Catal. A* **2005**, *279*, 79–88.

[13] a) S. Maheshwari, E. Jordan, S. Kumar, F. S. Bates, R. L. Penn, D. F. Shantz, M. Tsapatsis, *J. Am. Chem. Soc.* **2008**, *130*, 1507–1516; b) S. Maheshwari, C. Martínez, M. T. Portilla, F. J. Llopis, A. Corma, M. Tsapatsis, *J. Catal.* **2010**, *272*, 298–308.

[14] Q. Guo, F. Fan, E. A. Pidko, W. N. P. van der Graaff, Z. Feng, C. Li, E. J. M. Hensen, *ChemSusChem* **2013**, *6*, 1352–1356.

[15] a) G. Liu, J.-G. Jiang, B. Yang, X. Fang, H. Xu, H. Peng, L. Xu, Y. Liu, P. Wu, *Microporous Mesoporous Mater.* **2013**, *165*, 210–218; b) X. Ouyang, S.-J. Hwang, D. Xie, T. Rea, S. I. Zones, A. Katz, *ACS Catal.* **2015**, *5*, 3108–3119.

[16] a) C. Hammond, S. Conrad, I. Hermans, *Angew. Chem. Int. Ed.* **2012**, *51*, 11736–11739; *Angew. Chem.* **2012**, *124*, 11906–11909; b) C. Hammond, D. Padovan, A. Al-Nayili, P. P. Wells, E. K. Gibson, N. Dimitratos, *ChemCatChem* **2015**, *7*, 3322–3331.

[17] A. Corma, L. T. Nemeth, M. Renz, S. Valencia, *Nature* **2002**, *412*, 423–425.

[18] M. Renz, T. Blasco, A. Corma, V. Fornés, R. Jensen, L. Nemeth, *Chem. Eur. J.* **2002**, *8*, 4708–4717.

[19] H. Y. Luo, L. Bui, W. R. Gunther, E. Min, Y. Román-Leshkov, *ACS Catal.* **2012**, *2*, 2695–2699.

[20] M. Moliner, Y. Román-Leshkov, M. E. Davis, *Proc. Natl. Acad. Sci. USA* **2010**, *107*, 6164–6168.

[21] C. M. Osmundsen, M. S. Holm, S. Dahl, E. Taarning, *Proc. R. Soc. London Ser. A* **2012**, *468*, 2000–2016.

[22] P. I. Ravikovitch, A. V. Neimark, *Colloids Surf. A* **2001**, *187–188*, 11–21.

[23] a) S. Roy, K. Bakhmutsky, E. Mahmoud, R. F. Lobo, R. J. Gorte, *ACS Catal.* **2013**, *3*, 573–580; b) M. Boronat, P. Concepción, A. Corma, M. Renz, S. Valencia, *J. Catal.* **2005**, *234*, 111–118.

[24] a) O. M. Busch, W. Brijoux, S. Thomson, F. Schüth, *J. Catal.* **2004**, *222*, 174–179; b) B. Chakraborty, B. Viswanathan, *Catal. Today* **1999**, *49*, 253–260; c) F. de Clippel, M. Dusselier, R. Van Rompaey, P. Vanelderen, J. Dijkmans, E. Makshina, L. Giebeler, S. Oswald, G. V. Baron, J. F. M. Denayer, P. P. Pescarmona, P. A. Jacobs, B. F. Sels, *J. Am. Chem. Soc.* **2012**, *134*, 10089–10101.

[25] N. K. Mal, V. Ramaswamy, P. R. Rajamohanan, A. V. Ramaswamy, *Microporous Mater.* **1997**, *12*, 331–340.

[26] S. P. Elangovan, K. Inoue, T. Okubo, A. Kojima, M. Ogura, *Ind. Eng. Chem. Res.* **2007**, *46*, 1039–1044.

[27] V. Narkhede, H. Gies, *Chem. Mater.* **2009**, *21*, 4339–4346.

[28] S. Saravanamurugan, M. Paniagua, J. A. Melero, A. Riisager, *J. Am. Chem. Soc.* **2013**, *135*, 5246–5249.

[29] L. Ren, Q. Guo, P. Kumar, M. Orazov, D. Xu, S. M. Alhassan, K. A. Mkhoyan, M. E. Davis, M. Tsapatsis, *Angew. Chem. Int. Ed.* **2015**, *54*, 10848–10851; *Angew. Chem.* **2015**, *127*, 10998–11001.

[30] R. Bermejo-Deval, M. Orazov, R. Gounder, S.-J. Hwang, M. E. Davis, *ACS Catal.* **2014**, *4*, 2288–2297.

[31] a) Y. Román-Leshkov, M. Moliner, J. A. Labinger, M. E. Davis, *Angew. Chem. Int. Ed.* **2010**, *49*, 8954–8957; *Angew. Chem.* **2010**, *122*, 9138–9141; b) R. Bermejo-Deval, R. S. Assary, E. Nikolla, M. Moliner, Y. Román-Leshkov, S.-J. Hwang, A. Palsdottir, D. Silverman, R. F. Lobo, L. A. Curtiss, M. E. Davis, *Proc. Natl. Acad. Sci. USA* **2012**, *109*, 9727–9732.

[32] R. Bermejo-Deval, R. Gounder, M. E. Davis, *ACS Catal.* **2012**, *2*, 2705–2713.

Received: January 30, 2016
Published online on March 23, 2016